Amidinium-templated 2D [MnCr] Bimetallic Oxalate-Based Networks: The Influence on Structure and Magnetism Explored by Combining Experience and Theory

Catalin Maxim,[a,b,c] Sergi Saureu,[d,e] Coen de Graaf, [e,g] Sylvie Ferlay,[a,f,*] Mir Wais Hosseini,[a,f,] Vincent Robert[e,*] and Cyrille Train[b,f,*]

[a] *Molecular Tectonic Laboratory, UMR UDS-CNRS 7140, Université de Strasbourg, Institut Le Bel, 4, rue Blaise Pascal, F-67000 Strasbourg, France*

[b] *Laboratoire National des Champs Magnétiques Intenses, UPR CNRS 3228, 25 rue des Martyrs, B.P. 166, 38042 Grenoble cedex 9, France*

[c] *University of Bucharest, Faculty of Chemistry, Inorganic Chemistry Laboratory, Str. Dumbrava Rosie nr. 23, 020464-Bucharest, Romania.*

[d] *Laboratoire de Chimie Quantique, UMR 7177, 1 rue Blaise Pascal 67000 Strasbourg, France*

[e] *Departament de Química Física i Inorgànica, Universitat Rovira i Virgili, Marcel·lí Domingo s/n, 43007 Tarragona, Spain*

[f] *Institut Universitaire de France (IUF)*

[g] *Institució Catalana de Recerca i Estudis Avançats (ICREA), Passeig Lluís Companys 23, 08010, Barcelona, Spain*

Abstract

Three X^{2+} bisamidinium dications are used as template for the formation of oxalate-based bimetallic [MnCr] compounds 1-3 of formula $X[Mn^{II}(CH_3OH)Cr^{III}(ox)_3]_2 \cdot nS$ (X^{2+} = $C_{14}N_4H_{20}^{2+}$ (cation A, compound 1), $C_{14}O_2N_4H_{20}^{2+}$ (cation B, compound 2), $C_{16}N_4H_{24}^{2+}$ (cation C, compound 3); n=4 (1-2), 2 (3); S= CH_3OH (1-2), CH_3CN (3)). The single-crystal X-rays analysis reveals that in 1-3, a Mn-Cr oxalate-bridged bimetallic coordination network is formed, displaying corrugated two-dimensional (2D) layers based on heptacoordinated manganese(II) ions, with six oxygen atoms from three bis(bidentate) oxalate ions and one oxygen atom from a coordinated methanol molecule in the coordination sphere. In all cases, the coordination environment of manganese(II) is close to a Capped Trigonal PRism (CTPR). This evolution is related to the disymmetrization of one of the three oxalate linkages. Measurements of the magnetic properties revealed a continuous increase of the $\chi_M T$ product, where χ_M is the magnetic susceptibility, when the temperature is lowered from 300K to 5K, indicating the presence of a dominant ferromagnetic interaction in 1-3. The Curie-Weiss temperatures deduced from the fit of the magnetic susceptibility in the paramagnetic phase are 5.87K, 4.40K and 3.98K for 1, 2 and 3 respectively. From a mean field approach, an average weak ferromagnetic exchange interaction of 0.62K, 0.42K and 0.54K respectively can be deduced. *Ab initio* calculations up to the DDCI-2 level were performed on [MnCr] dimeric units. They allow to evaluate the exchange interaction for each type of bridges present in the three compounds. An effect of the asymmetry of the bridge on the exchange interaction is observed but not in a systematic way.

Introduction

Since their discovery,[1] the synthesis of oxalate-based bimetallic networks was rationalised following a sorting into two "robust" categories: (10,3) three-dimensional (3D) networks and (6,3) three-dimensional (2D) networks[2] displaying a large variety of magnetic properties when paramagnetic metals are used: magneto-chiral dichroism[3] or magnetisation-induced second harmonic generation,[4] for example. Few exceptions to these architectures and stoechiometries were presented in the literature and were considered as exotic cases,[5,6] that did not invalid the general scheme of synthesis. Recently, to favour the appearance of new properties under electric field,[7,8,9,10] cations with H-bonding abilities were introduced as templating agents in the anionic oxalate-based [MnCr] bimetallic coordination networks. It then appeared a competition between the formation of charge assisted hydrogen- and coordination bonds. The latter holding the anionic network, the insertion of such cations can deeply influence the nature of the formed coordination network[8-10] or even prevents its formation.[11,12,13] The evolutions of the [MnCr] bimetallic coordination network are essentially related to variations of the manganese(II) coordination environment and/or of the oxalate bridging mode. In parallel to these structural changes, modifications in the exchange interactions and Long Range Magnetic Ordering (LRMO) were observed. In particular, a dramatic change from ferromagnetic to antiferromagnetic of the Mn(II)-Cr(III) S=5/2 and S=3/2 exchange interaction was tentatively attributed to the sweeping from a bisbidentate to a bidentate/monodentate bridging mode of the oxalate ligand.[14] This influence of the bridging mode of the oxalate must be experimentally further investigated and theoretically confirmed to be validated. For this purpose, using the template effect induced by cationic organic species incorporated in a [MnCr] bimetallic network appears an appealing strategy.

Amidinium-containing cations have already shown the ability to form supramolecular hydrogen bonded networks with

the oxalate bridged system.[15] In addition, they have lead to a large variety of functional hydrogen bonded systems.[16,17] Along these lines, the synthesis, structure and magnetic properties of three [MnCr] oxalate-based compounds obtained by using three different amidinium-based cations, namely 1,4-bis(1,4,5,6-tetrahydropyrimidinium-2-yl)benzene ($\mathbf{A}^{2+}$), 2,2'-(1,4-phenylene)bis(1,4,5,6-tetrahydropyrimidinium-5-ol) ($\mathbf{B}^{2+}$) and 1,4-bis(1-methyl-1,4,5,6-tetrahydropyrimidinium-2-yl)benzene ($\mathbf{C}^{2+}$) (Scheme 1) are presented. The obtained compounds present all the same Mn/Cr ratio as well as an analogous hepta coordination of the Mn(II) centres, with the following formula $X[Mn^{II}(CH_3OH)Cr^{III}(ox)_3]_2 \cdot nS$ (X^{2+} = $C_{14}N_4H_{20}^{2+}$ (**1**), $C_{14}O_2N_4H_{20}^{2+}$ (**2**), $C_{16}N_4H_{24}^{2+}$ (**3**); n=4 (**1-2**), 2 (**3**); S= CH_3OH (**1-2**), CH_3CN (**3**)). The structural data are used as a solid basis to perform a thorough *ab initio* theoretical study to establish a possible magneto-structural correlation between the geometry of the oxalate bridge and the exchange interaction between the metallic centres.

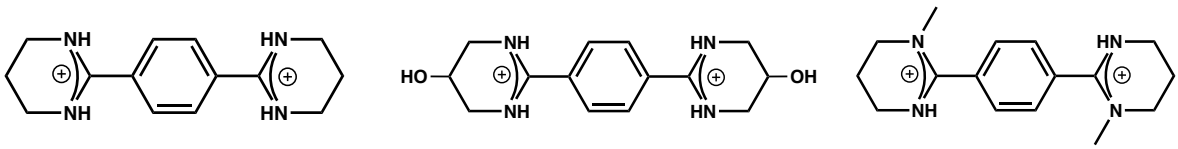

$\mathbf{A}^{2+}$ $\mathbf{B}^{2+}$ $\mathbf{C}^{2+}$

Scheme 1. Amidinium-based dications templating the formation of the oxalate-based compounds.

Experimental part

Synthesis

$MnCl_2 \cdot 4H_2O$ was purchased from commercial sources and used as received. $(NH_4)_3[Cr(ox)_3] \cdot 3H_2O$,[18] $\mathbf{A}Cl_2$,[19] $\mathbf{B}Cl_2$[18] and $\mathbf{C}Cl_2$,[20] (Scheme 1) were prepared following the published procedures.

Synthesis of 1, 2 and 3:

$\mathbf{A[Mn^{II}(CH_3OH)Cr^{III}(ox)_3]_2 \cdot 4CH_3OH}$ (1). $(NH_4)_3[Cr(ox)_3] \cdot 3H_2O$ (85.6 mg, 0.2 mmol) and $MnCl_2 \cdot 4H_2O$ (40 mg, 0.2 mmol) in 8 mL methanol was introduced in a 1.5 cm diameter tube and layered with 15 mL CH_3OH. A methanolic solution (3mL) containing $\mathbf{A}Cl_2$ (25 mg, 0.1 mmol) was then layered. After 2-3 days, violet crystals were formed at the interface. Elemental analysis calculated (%) for $C_{32}H_{44}Cr_2Mn_2N_4O_{30}$ (1178.6): C 32.61, H 3.76, N 4.75; found: C 31.58, H 3.36, N 4.28; IR: ν = 3457 (O-H), 3124 (N–H), 3035 and 2990 (C–H), 1701, 1659, 1640 cm^{-1} (C–O).

$\mathbf{B[Mn^{II}(CH_3OH)Cr^{III}(ox)_3]_2 \cdot 4CH_3OH}$ (2). $(NH_4)_3[Cr(ox)_3] \cdot 3H_2O$ (85.6 mg, 0.2 mmol) and $MnCl_2 \cdot 4H_2O$ (40 mg, 0.2 mmol) in 8 mL methanol was introduced in a 1.5 cm diameter tube and layered with 12 mL CH_3OH. A methanolic solution (4mL) containing $\mathbf{B}Cl_2$ (20 mg, 0.1 mmol) was then layered. After 3 days, violet crystals were formed at the interface. Elemental analysis calculated (%) for $C_{32}H_{44}Cr_2Mn_2N_4O_{32}$ (1210.65): C 31.74, H 3.66, N 4.62; found: C 31.18, H 3.24, N 4.32; IR: ν = 3459 (O-H), 3120 (N–H), 3025 and 2989 (C–H), 1702, 1657, 1639 cm^{-1} (C–O).

$\mathbf{C[Mn^{II}(CH_3OH)Cr^{III}(ox)_3]_2 \cdot 2CH_3CN}$ (3). Compound **3** was obtained as violet crystals by slow evaporation at room temperature (1 day) of an solvent mixture solution (5 mL $CH_3OH/CH_3CN/H_2O$ 4:4:1) containing $(NH_4)_3[Cr(ox)_3] \cdot 3H_2O$ (52.5 mg, 0.125 mmol), $MnCl_2 \cdot 4H_2O$ (25 mg, 0.125 mmol) and $\mathbf{C}Cl_2$ (27 mg, 0.063 mmol). Elemental analysis calculated (%) for $C_{34}H_{38}Cr_2Mn_2N_6O_{26}$ (1260.55): C 35.18, H 3.30, N 7.24; found: C 35.05, H 3.18, N 7.14; IR: ν = 3447 (O-H), 3114 (N–H), 3015 and 2988 (C–H), 1703, 1649, 1638 cm^{-1} (C–O).

Characterization techniques

FT-IR spectra were recorded on a Perkin Elmer ATR spectrometer.

Microanalyses were performed by the shared Elemental Analysis Service at Université de Strasbourg.

TGA measurements have been performed on polycrystalline compounds on Pyris 6 TGA Lab System (Perkin-Elmer), using a N_2 flow of 20 mL/mn and a heat rate of 4°C/mn.

Variable temperature (2.0-300 K) magnetic susceptibility measurements were carried out on polycrystalline samples with a MPMS SQUID magnetometer by applying a 1000 G external magnetic field.

Structural studies

Single-Crystal Studies

Data were collected at 173(2) K on a Bruker APEX8 CCD Diffractometer (compound **2** and **3**) equipped with an Oxford Cryosystem liquid N_2 device, using graphite-monochromated Mo-Kα (λ = 0.71073) radiation and on Xcalibur E Diffractometer (compound **1**) using Cu-Kα (λ = 1.54184) radiation. The structures were solved by direct methods and refined by full-matrix least squares techniques based on F^2. The non-H atoms were refined with anisotropic displacement parameters. Calculations were performed using SHELX-2013 crystallographic software package. All

hydrogen atoms were generated geometrically.[21] For compound **2** the noncoordinated methanol molecules are highly disordered which could not be located successfully from Fourier maps in the refinement cycles. The scattering from the highly disordered lattice guest molecules were removed using the SQUEEZE procedure implemented in the PLATON package[22]. Moreover, the coordinated methanol molecules are disordered over two positions, with a ratio refined at 0.67:0.33.
CCDC 1448152-1448154 contain supplementary crystallographic data for the three compounds. They can be obtained free of charge from the Cambridge Crystallographic Data Centre via www.ccdc.cam.ac.uk/datarequest/cif.

Powder diffraction studies (PXRD)

Diagrams were collected on a Bruker D8 diffractometer using monochromatic Cu-Kα radiation with a scanning range between 4 and 40° using a scan step size of 8°/mn.
As already demonstrated and currently admitted, for all compounds, discrepancies in intensity between the observed and simulated patterns are due to preferential orientations of the microcrystalline powders.

Computational details

For each compound, three different Mn(μ-ox)Cr pairs were considered using the anionic units represented in Fig. 1. The geometrical parameters extracted from the different crystal structures were applied without performing any further geometry optimization. The presence of five unpaired electrons on high-spin Mn(II) and three on the Cr(III) ion leads to a 8-electron 8-orbital complete active space, denoted as CAS(8,8). The orbitals and configuration expansion coefficients of the S = 1, 2, 3 and 4 wave functions were optimized to minimize the energy for all twelve units in a CASSCF (complete active space self-consistent filed) framework. It has been clearly demonstrated that a bare valence-only description is not sufficient to grasp energy differences in spin-coupled systems.[23,24] Thus, dynamic electron correlation contributions were then incorporated using the difference dedicated configuration interaction (DDCI) method as implemented in the CASDI code.[25,26] The DDCI approach aims at hierarchizing different states, which share similar spatial descriptions. Therefore, one has to choose a common set of molecular orbitals (MO) to build up the CI space. The CAS(8,8)SCF nanuplet MOs were used throughout the spin states energies evaluation. The CAS(8,8)SCF wave function is used as reference and depending on the number of holes created in the doubly occupied (inactive) and particles created in the empty (virtual) orbitals, the resulting CI space can be labelled as DDCI-1, DDCI-2 and DDCI-3.[27] All the results in this work refer to DDCI-2. Given the large number of determinants in the reference wave function, the straightforward application of the DDCI approach leads to an unmanageably large wave function expansion. Therefore, we have followed two different approaches to keep the calculation tractable. In the first place, the delocalized molecular orbitals of the S=4 state were transformed to a set of localized orbitals,[28] which can be classified by there shape as core orbitals, σ, σ*-orbitals, π, π*-orbitals, etc. This procedure allows us to split the system following a valence bond-like picture, staying in an orthogonal framework. The method has proven to be extremely efficient not only to reduce in a rational way the number of inactive and virtual MOs in post CASSCF treatments but also to analyse the relevance of chemical regions in energy differences.[29] The procedure is particularly attractive in exchange coupling constants calculations since one can concentrate the numerical efforts according the polarizable nature of the different fragments. The DOLO program (implemented in CASDI code) was used to perform the localization procedure. The second, complementary reduction step consist in eliminating all the deadwood configurations from the reference wave function. For this purpose, we only kept the neutral (Cr^{3+}-Mn^{2+}) and ionic (Cr^{4+}-Mn^{+} and Cr^{2+}-Mn^{3+}) configurations, while all the di- and tri-ionic configurations were eliminated from the CASSCF wave function.[30]. This classification of the configurations in the CAS wave function can only be made when the active orbitals are localized on the magnetic centres as shown in figure 1.

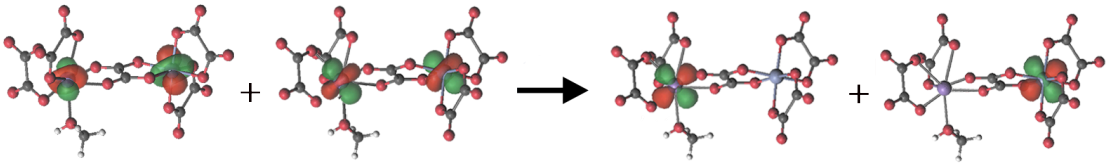

Figure 1. Example of the localization procedure. The molecular orbital on the left is non-localized (a mixture of the MOs of the 2 metal centres) and the molecular orbitals of the right are the localized after DOLO program procedure.

Extended basis sets were used for the metal centres and nearest-neighbour oxygen atoms, namely ANO-RCC 5s4p2d1f and 3s2p1d. The other oxygen and carbon atoms were described with ANO-RCC 2s1p, while the H atoms were assigned a 2s basis set. All our calculations were performed using the MOLCAS suite of program[31] and subsequent CASDI chain.[25]

Results and discussion

Synthesis

Compounds **1** and **2** were obtained as crystalline materials by slow evaporation at room temperature of a methanolic solution containing tris(oxalato)chromate(III) and manganese(II) chloride and the chloride salt of the template cation ($\mathbf{A}^{2+}$ and $\mathbf{B}^{2+}$). Compound **3** was obtained following the same procedure (with $\mathbf{C}^{2+}$), but using a $CH_3OH/CH_3CN/H_2O$ mixture. For the three compounds, PXRD (Fig. ESI1) and TGA measurements (fig. ESI2) of the polycrystalline samples demonstrates that a single compound is formed during the crystallization process and that the number of solvent molecules found in the polycrystalline powder fits well with the one found by XRD (4 CH_3OH for **1** and **2** and CH_3CN for **3**).

As already mentioned, in **1**-**3**, methanol used as solvent appears to be coordinating to Mn(II). This was previously observed in 2D oxalate-based networks when methanol or ethanol are used as solvents.[9,14] As demonstrated below by single-crystal diffraction, the tris(oxalate)chromate(III) is preserved during the self-assembly process and the oxalate ligand act as a bisbidentate ligand. The introduction of H-bond active cations leads to numerous directional hydrogen bonds between the coordination network and the organic cation present in the crystal. This contrasts with the "standard" oxalate-based networks[2] but was previously observed with other H-bond active cations leading to distortion of the coordination network or even to a lowering of the dimensionality of the coordination architecture to isolated complexes.[8-13] In the present cases, the implication of the oxygen atoms of oxalate ligands in hydrogen bonds weakens their coordination ability towards manganese(II) allowing the coordination of an extra monodentate ligand available in solution, *e.g.* a methanol molecule.

Structural description

1 and **2** revealed to be isomorphous (monoclinic, $P2_1/c$) and also isometric (cell parameter in the same range), so both compounds are isostructural. **3** displays a slightly different packing. In all the compounds, the asymmetric unit is based on one half of an amidinium dication lying about an inversion centre with one anionic dimeric units $[(CH_3OH)Mn^{II}(ox)Cr^{III}(ox)_2]^-$ and solvent molecules. Their formula are $\mathbf{A}[Mn^{II}(CH_3OH)Cr^{III}(ox)_3]_2{\cdot}4CH_3OH$ for **1**, $\mathbf{B}[Mn^{II}(CH_3OH)Cr^{III}(ox)_3]_2{\cdot}4CH_3OH$ for **2** and $\mathbf{C}[Mn^{II}(CH_3OH)Cr^{III}(ox)_3]_2{\cdot}2CH_3CN$ for **3** (figure 2).

Table 1. Crystallographic parameters for compounds **1-3** $^aR_1 = \sum||F_o|-|F_c||/\sum|F_o|$. $^bwR_2 = [\sum w(F_o^2 - F_c^2)^2/\sum w(F_o^2)^2]^{1/2}$; $w = 1/[\sigma^2(F_0^2)+(aP)^2+bP]$ where $P= [\max(F_0^2, 0) + 2F_c^2]/3$.

	1	**2**	**3**
Formula	$C_{16}H_{22}CrMnN_2O_{15}$	$C_{14}H_{14}CrMnN_2O_{14}$	$C_{17}H_{19}CrMnN_3O_{13}$
Molecular weight	589.29	541.21	580.29
Crystal system	monoclinic	monoclinic	monoclinic
Space group	P21/c	P21/c	P21/n
a(Å)	8.9951(3)	8.9291(4)	9.2235(2)
b(Å)	16.2549(3)	16.1789(8)	15.3552(4)
c(Å)	15.2284(3)	16.5533(8)	16.5639(5)
β(deg)	98.070(2)	103.8590(10)	100.7650(10)
V(Å^3)	2204.56(10)	2321.72(19)	2304.64(10)
Z	4	4	4
Colour	violet	violet	violet
Dcalc (gcm^{-3})	1.775	1.548	1.672
F(000)	1204	1092	1180
μ (mm-1)	9.482	1.103	1.091
Wavelength (Å)	1.54184	0.71073	0.71073
Number of data meas.	15002	13145	16771
Number of data with I> 2σ(I)	4079 [R(int) = 0.0393]	4078 [R(int) = 0.0252]	4014 [R(int) = 0.0371]
Final R_1[a],wR_2 [b][I>2σ(I)]	R1 = 0.0424, wR2 = 0.1208	R1 = 0.0344, wR2 = 0.0867	R1 = 0.0505, wR2 = 0.1232
R_1 [a], wR_2 [b](all data)	R1 = 0.0471, wR2 = 0.1338	R1 = 0.0375, wR2 = 0.0887	R1 = 0.0606 wR2 = 0.1303
GOF	1.086	1.070	1.113
Largest peak in final difference (eÅ^{-3})	-0.700, 0.934	-1.204, 0.500	-0.599, 0.648

Compounds **1-3** are displaying a lamellar structure where the $[(CH_3OH)Mn^{II}(ox)Cr^{III}(ox)_2]^-$ anionic units are forming bimetallic honeycomb pseudo-hexagonal layers, with alternating Cr(III) and Mn(II) centres, parallel to the *ab* plane (Figure 3). This is consistent with the structures observed in many bimetallic 2D oxalate-bridged systems.[2] In these bimetallic planes, the environment of the metal ions are comparable within the series as well as in a previously described compound of $[Mn(CH_3OH)_6][MnCr(ox)_3CH_3OH]\cdot 2CH_3OH$,[14] thereafter numbered **4** and structures of **1-3** will always be compared to this latter.

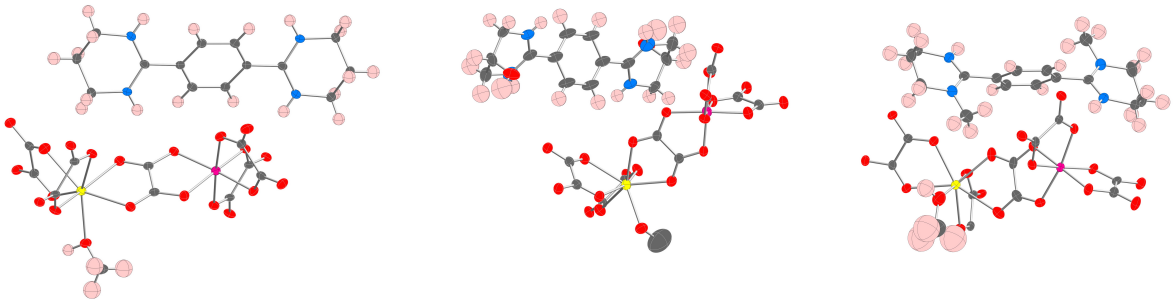

1 **2** **3**

Figure 2. Dicationic and anionic units forming compounds **1-3** and their thermal ellipsoid representation.

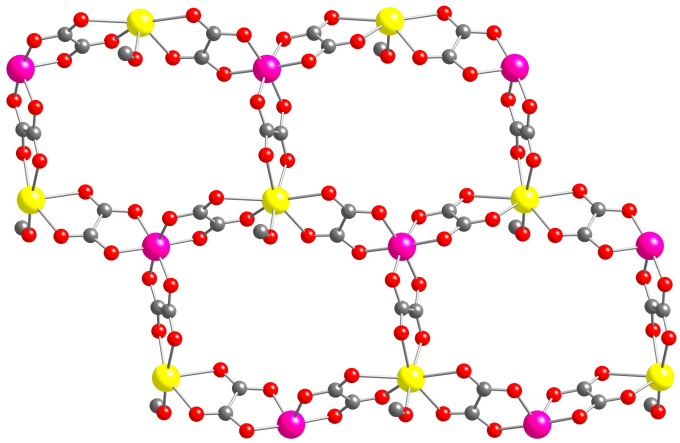

Figure 3. The deformed bimetallic honeycomb pseudo-hexagonal anionic system in compounds **1-3** in plane observed for **3**. The heptacoordination of Mn(II) (in yellow) is represented). Cr(III) cations in pink.

In all four compounds and as already said, the Cr(III) ions are in an octahedral environment with Cr-O distances in a narrow range and consistent to with the previous observations (Table 2). Within a given layer, all the Cr(III) helical centres present the same absolute configuration whereas, following the observed space groups, the opposite configuration is observed in the adjacent layers leading to an overall achiral structure. In contrast, the Mn(II) ions adopt an heptacoordinated environment where Mn-O distances (Table 2) and O-Mn-O angles undergo impressive variations compared to the idealized coordination polyedra in heptacoordination,[32] *e.g*. Capped OCtahedron (COC-7), Capped Trigonal PRism (CTPR-7) and PentagonalBiPYramid (PBPY-7). Continuous Shape Measurements (CSM) thus appear as the best instrument to describe the coordination environment of the heptacoordinated manganese(II) centers. The CSM values (Table 2) for compounds **1-4** indicate that the closest idealized coordination polyhedron is CTPR-7 for the four compounds. In the case of **1** and **3**, the difference with PBPY-7 and COC-7 respectively is small, indicating that the coordination polyhedron adopts an intermediate geometry, which is also the case for compound **4**. For two of the three chelating oxalate ligands, the difference between the two Mn-O(ox) distances is in a 0-5% range leading to a rather symmetrical positioning of the ligand. The situation is dramatically different for the third oxalate ligand. In all cases, it exhibits the shortest and the longest Mn-O(oxalate) distances, which is the expression of the dissymmetry of the oxalate ligand. The ratio between the two distances goes from 0.92 for **2** down to 0.77 for **4**. In the latter case, with a Mn-O(oxalate) long distance of 2.813 Å, the authors actually did not even consider the presence of a second coordination bond between the third oxalate ligand and the Mn(II) ion.[14]

Table 2. Relevant angles and distances in **1-4**. The data for **4** are extracted from ref. 14 and also values obtained for **1-4** after CSM

	1	**2**	**3**	**4**[14]
Cr-O	1.976(3)-2.011(3)	1.967(2)-1.984(2)	1.959(4)- 1.984(3)	1.954(3)- 1.986(3)
Mn-O (oxalate)	2.176(3)-2.462(3)	2.193-2.391(2)	2.192(4)- 2.513(4)	2.159(3)-2.814(3)
Mn-O (MeOH)	2.224(3)	2.256(3)	2.148(3)	2.138(3)
N…O (Cation-oxalate)	2.817-3.074	2.905-3.275	3.252	-
O…O (MeOH)	2.853-3.009	3.084-3.179	-	-
	CSM for Mn(II)			
S(MnO_7) to COC-7	3.67	3.35	2.68	3.77
S(MnO_7) to CTPR-7	**2.05**	**1.78**	**2.18**	**2.44**
S(MnO_7) to PBPY-7	2.69	2.96	3.03	3.55

The non-octahedral environment of the Mn(II) ions induces a bending of the Mn-Cr motives. Due to the presence of the inversion centres, this leads to a corrugation of the bimetallic planes. In **3**, the planes are stacked one above the other whereas in **1** and **2**, the planes are staggered, leading to the formation of "pockets" where the dications and solvent molecules are located (Figure 4). The dicationic units are indeed connecting the anionic layers through charge assisted[33] N-H···O(ox) hydrogen bonds, ranging from 2.817 to 3.252Å (see table 2) between the dicationic units and the anionic layer. In **2**, the hydroxyle groups of the cations are also involved in H bonds as well as the crystallization methanol molecules (O-O bonds ranging from 2.853 to 3.179Å in **1** and **2**). In **3**, the acetonitrile molecules are interacting with the oxygen atoms from the oxalate ligands through hydrogen bonds (Table 2).

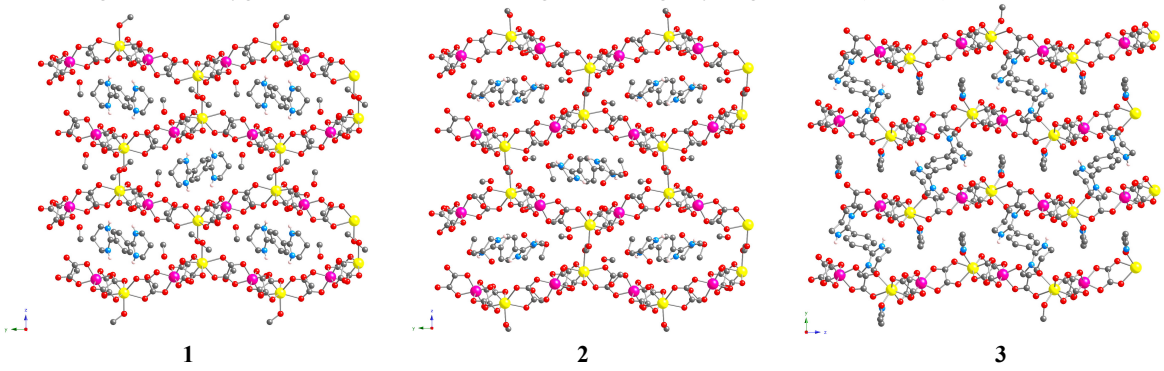

Figure 4. Dicationic and anionic units in compounds **1-3**, enhancing the corrugated character of the layers, together with the location of the dication between them.

Magnetic properties

For compounds **1-3**, the thermal evolution of the $\chi_M T$ product and χ_M^{-1} are shown in Figure 5. The magnetic behaviour of the three compounds appears as very similar despite the structural changes stated above. At room temperature, the $\chi_M T$ values are 6.35 (**1**), 6.46 (**2**) and 6.28 $cm^3.mol^{-1}.K$ (**3**). They are close to those expected for the sum of the corresponding non-interacting metal ions (6.25 $cm^3\ mol^{-1}$ K considering g=2.00 for both metal ions). Upon cooling, the $\chi_M T$ product for **1-3** increases continuously. This evolution is indicative that the exchange interactions between the two metal(II) ions are dominated by ferromagnetic ones.

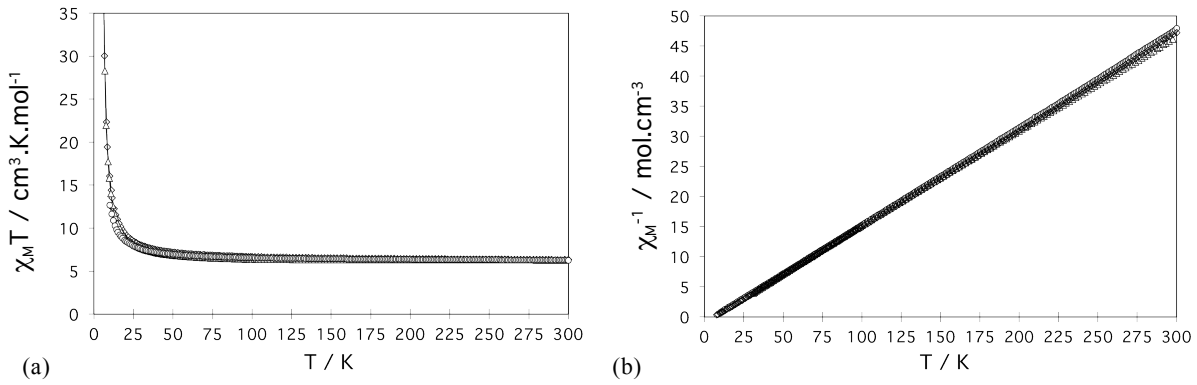

Figure 5. Thermal variation of the $\chi_M T$ product (a) and the inverse magnetic susceptibility χ_M^{-1} (b) for compound **1** (diamonds), **2** (trinagles) and **3** (circles).

To quantify the average interaction, the inverse susceptibility (figure 5b) is fitted using a Curie-Weiss law to determine the Curie-Weiss temperatures given in Table 3. In a mean field approach, the Curie-Weiss temperature Θ can be related to the exchange interaction J.[34] In most cases,[34,35] a unique exchange interaction parameter is taken for a given pair of metal ions. In the present case, the structural analysis indicates that there are strong structural differences between the three oxalate bridges. It is therefore necessary to introduce three different exchange interaction parameters J_1, J_2 and J_3 for the three types of oxalate bridges present in the three compounds (see Figure 6) At this stage, let us stess that no attribution can be made and subsequent theoretical inspections should complement this picture.

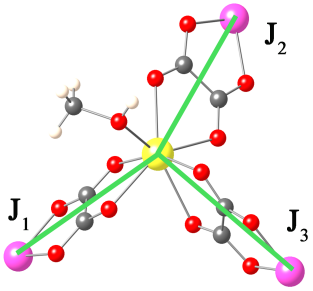

Figure 6. Schematic representation of the 3 different magnetic pathways in the hexagonal layers formed by the anionic units. The attribution of J_1, J_2 and J_3 to the three different pairs is arbitrary but aims at stressing the existing structural differences within each compound.

The relationship between the Curie-Weiss temperature and the exchange parameters is then:

$$\Theta = 4\cdot(J_1+J_2+J_3)/3 \cdot S_{Mn^{II}}(S_{Mn^{II}}+1)S_{Cr^{III}}(S_{Cr^{III}}+1)/(S_{Mn^{II}}(S_{Mn^{II}}+1)+S_{Cr^{III}}(S_{Cr^{III}}+1)) \qquad \text{(eq. 1.1)}$$

$$\Theta = 4\cdot\langle J\rangle \cdot S_{Mn^{II}}(S_{Mn^{II}}+1)S_{Cr^{III}}(S_{Cr^{III}}+1)/(S_{Mn^{II}}(S_{Mn^{II}}+1)+S_{Cr^{III}}(S_{Cr^{III}}+1)) \qquad \text{(eq. 1.2)}$$

where S_i is the spin value of the metal center i S=5/2 and S=3/2.

Nevertheless, as expected from a mean field approach, the Curie-Weiss temperature is proportional to the arithmetic mean of the three exchange parameters. In contrast with the approach proposed by Ohkoshi *et al*. on ternary Prussian Blue Analogues,[35] it is not possible to go further in the present case because these compounds are made of only two independent magnetic subnetworks. The average $\langle J\rangle_{exp}$ deduced from eq. 1.2 are gathered in Table 3.
In ref. 14, the authors have tentatively related the extreme lengthening of one the Mn-O coordination bond in compound **4** with the appearance of antiferromagnetic coupling. This proposal was natural when considering the seminal work on oxalate-bridged dicopper(II) complexes where the modifications of the bridge definitely led to strong modifications of the overlap between the magnetic orbitals and, following Kahn's model, to impressive modification of the exchange interaction.[36] Nevertheless, within the presented series, this explanation does not seem to hold since compound **3** is the compound where the deformation of one of the three bridges is the most severe but the weakest average exchange interaction is found for **2**. The variations of the average exchange interaction parameter do not correlate with the CSM for the manganese(II) center neither. Is the averaging of the three exchange interaction constants masking the appearance of an antiferromagnetic contribution for the most dissymmetrical bridge? A theoretical inspection where the three bridges are treated independently might be able to answer this question.

Table 3. Experimental and theoretical magnetic parameters for compounds **1-4**. For **4**, the Curie-Weiss temperature is taken from ref.14.

	1	**2**	**3**	**4**
Θ / K	5.87	4.40	5.67	-9.90
$\langle J\rangle_{exp}$ / K	0.61	0.42	0.54	-0.94

Ab initio Calculations

Quantum chemistry calculations were performed to explore the nature and magnitude of the exchange interactions for the three different Mn(μ-ox)Cr pairs (Figure 6) present in compounds **1-4** (Figure 7). In all cases, the Mn(μ-ox)Cr magnetic core is preserved but the geometry of the bridge differs. Considering that these pair interactions are not accessible independently from the experiment, the theoretical exploration should complement the magnetic measurements and finely stress the

influence of the characteristics of the Mn(II) coordination sphere and of the oxalate bridge on the exchange interaction parameters. Our goal is to quantify the possible deviation between the three constants within a given compound and to look for a trend in the series of compounds.

The localization procedure allows us to only include in the construction of the DDCI space those orbitals that are important for the electron correlation, and hence for the energy differences among the different spin states. From the occupied orbitals, all core orbitals were frozen whereas the bonding σ and π-types MOs were included in the treatment of the electron correlation. Naturally, the Cr and Mn 3d orbitals were included in the active space since they define the co-called minimal active space. The virtual MOs were divided in two groups. The first consisted of the σ*- and π*-orbitals extended with the Cr and Mn 4d. The 4d orbitals ensure a balanced description of the dynamic electronic correlation associated to the Cr/Mn orbitals. The second group contains all other virtual orbitals, all with a rather diffuse character. Only the first group of virtual orbitals was considered, the diffuse orbitals were deleted. An overview of the difference classes of orbitals is given in Table 4.

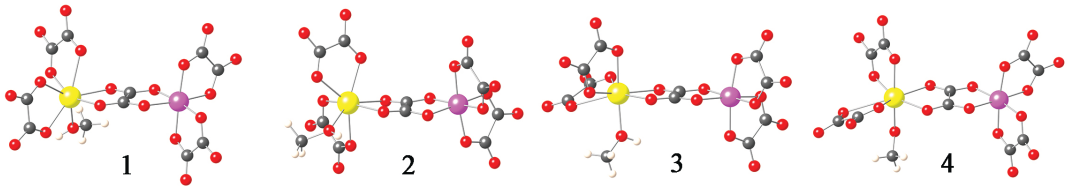

Figure 7. A Mn(μ-ox)Cr representative of the twelve structures obtained from the crystal structures used for the computational studies.

Table 4. Schematic representation of the orbitals used on the DDCI calculation

	n Orbitals (type)
Frozen	50 (core)
Inactive	96 (σ + π)
Active	8 (d-Mn + d-Cr)
Virtuals	52 (d'-M + σ* + π*)
Deleted	151 (others)

Table 5. Extracted coupling constants from CAS[8,8] + DDCI-2 calculations in compounds **1-4**. These values are related to the three oxalate-bridged Mn-Cr pairs identified by the Mn-O(ox) distances (Å) given in parenthesis.

	1	**2**	**3**	**4**
J_{1th} / K	0.27 (2.17-2.46)	0.21 (2.19-2.39)	0.26 (2.19-2.51)	0.08 (2.16-2.81)
J_{2th} / K	0.24 (2.27-2.20)	0.38 (2.27-2.28)	0.28 (2.25-2.35)	0.43 (2.18-2.22)
J_{3th} / K	0.46 (2.22-2.30)	0.45 (2.20-2.28)	0.29 (2.22-2.25)	0.53 (2.26-2.30)

Table 5 summarizes the CAS[8,8] + DDCI2 calculations and exchange coupling constants performed on the three Mn(μ-ox)Cr pairs of compounds **1-4**. The reported values are averages performed on the three spin state energy differences (S=1, 2, 3 and 4, resulting from the S_{MnII} = 5/2 and S_{CrIII} = 3/2 coupling). First, we observed that the latter follow the expected Heisenberg behaviour E(S-1) - E(S) = J·S with deviations smaller than 1.5%. Therefore, the description of the magnetic properties of each individual pair by means of a Heisenberg Hamiltonian is fully justified. Let us stress that important deviations to Heisenberg picture have been observed and rationalized for S > 1/2 spin-coupled systems.[37,27] Then, the calculated values are all positive, a reflection of the ferromagnetic behaviour in all considered pairs. This observation is somewhat puzzling since an antiferromagnetic behaviour was reported in compound **4**.

Let us therefore further analyse the results obtained for the three types of bridges. The asymmetry in the two Mn-O(ox) distances is largest for J_1 (see Table 5). Despite the relatively small amplitude of the exchange coupling constants, one can observe a general trend favouring a smaller J_1 value for a larger asymmetry character. This is most pronounced when compounds **1, 2, 3** are compared to compound **4**. Indeed, the nearly monodentate coordination in **4** leads to a very weak J_1 value that, however, is suggestive of ferromagnetic behaviour. Hence, we can confirm on the importance of the asymmetry of the Mn-oxalate coordination on the magnetic coupling. Accordingly, J_2 and J_3 exhibit comparable amplitudes in all four

complexes, and so are all the Mn-O(ox) distances (see Table 5). Finally, in order to address the influence of the methanol coordination on the coupling, we have evaluated the magnetic coupling in a related Mn(μ-ox)Cr compound synthesized without the presence of methanol. The resulting magnetic units show nearly regular octahedral coordination spheres around Mn and Cr. The calculated exchange coupling constants are between 0.4-0.8 K for the three different pathways, in line but slightly larger to those listed in Table 5. This increase can be related to average Mn-O distances about 0.2 Å smaller than in the compounds where manganese(II) is heptacoordinated.

From our calculations, it appears that the asymmetry of the bridge does have an influence on the magnetic coupling but does not provide a clear-cut explanation in the nature and amplitude of the experimental observations (see Table 3). The calculated and experimental exchange interaction parameters have the same magnitude but the contributions of J_2 and J_3 blurs out the small differences observed on J_1. One may question the procedure that consists in averaging over the three pathways (see Figure 6), positive values J_1, J_2 and J_3 suggesting a ferromagnetic behaviour in all **1-4** compounds.

Thus one may use a different strategy to make contact with experimental observations. Setting the S=2 energy to zero as a reference for all three pairs, one can average the three energies of spin states. Evidently, no dramatic change is expected as a consequence of the robustness of the Heisenberg picture. Nevertheless, this strategy follows the idea of having a single exchange interaction that reflects the occupations of averaged spin states. The calculated energies are given in Table 6, and as expected, a ferromagnetic behaviour is preserved in all compounds. It should be noted that the reverse problem was observed for DFT calculations performed on trinuclear oxalate-bridged complexes.[12]

Table 6. Average energies (K) of the different spin states and geometries calculated at the CAS[8,8] + DDC2 level. The nanuplet S=4 energy has been chosen as reference.

	1	**2**	**3**	**4**
S=4	0.00	0.00	0.00	0.00
S=3	2.59	2.78	2.24	2.81
S=2	4.47	4.81	3.88	4.84
S=1	5.80	6.23	5.02	6.27
$\mathbf{J_{avg}}$	0.32	0.35	0.28	0.35

This is indicative that the pair model where only the coordination bonds between the two metal centers are considered, which is the basis of most exchange parameter analysis in molecular magnetism, may not capture all the physical effects in extended materials. In turn, charge repartition,[38] H-bonding[39] and/or magnetic anisotropy should play a crucial role all the more that the observed coupling constants have a modest magnitudes. The latter parameter is explored in the four compounds by calculating the zero-field splitting (ZFS) parameters for the Cr(III) and Mn(II) centers (Table 6) following the strategy described in Ref. 40.[40] In all cases only a non-negligible axial anisotropy (D) appears, the rhombic anisotropy (E) being very small. Provided that the isotropic coupling between Cr(III) and Mn(II) dominates over the single ion anisotropy, the sublevels of the S=4 state can be described with an effective zero-field Hamiltonian[41] $S \cdot D(eff) \cdot S$, where D(eff) is $(3/28)D_{Cr} + (5/14)D_{Mn} = -0.29$ K. The S=3 state lies at 8J and the effective axial anisotropy becomes -0.14 K for this state. This means that the manifold of M_S sublevels of this spin state overlaps with the manifold of the S=4 state, and hence, the strong exchange assumption is probably not valid. This increases enormously the difficulty of the theoretical analysis of the magnetic properties as was shown by Maurice et al. in a study of a Ni dimer in the weak exchange limit.[42] In that complex it was also found that the isotropic coupling (ferromagnetic in nature) extracted from very precise ab initio calculations was slightly smaller than the one estimated from experimental data, exactly as in the present case. Concerning complex **4**, we tentatively assign the disagreement between theory (ferromagnetic isotropic coupling) and experiment (antiferromagnetic isotropic coupling) to the weak exchange regime, which makes the fitting of the magnetic susceptibility a delicate question.

Table 7. Calculated zero field splitting parameters D (axial) and E (rhombic) parameters (K) of the Cr and Mn centers in the four compounds.

	1		**2**		**3**		**4**	
	D	E	D	E	D	E	D	E
Cr	-0.95	0.04	-0.87	0.10	-0.64	0.04	-0.88	0.04
Mn	-0.53	0.07	-0.54	0.05	-0.41	0.06	-0.27	0.12
$\mathbf{J_{avg}}$	0.32		0.35		0.28		0.35	

Conclusion

The synthesis of compounds **1**-**3** confirms the ability of anionic 2D oxalate-bridged [MnCr] networks to welcome organic dications. They are indeed the first 2D compounds where dications are inserted whereas this result was discovered in the 1990's for 3D compounds.[43] In comparison with previous cases,[11,12] the competition between coordination and hydrogen bonds did not hinder the formation of the 2D coordination network but, as already observed,[9,14] it induced the corrugation of the layers because the manganese(II) centres are heptacoordinated, while using MeOH as solvent during the formation of the extended compounds. This phenomenon influences the magnetic exchange parameter between the metal-centres though the switch from a ferromagnetic to an antiferromagnetic interaction observed[14] in **4** was not observed experimentally nor reproduced theoretically. In the latter case, this raises fundamental questions about the phenomena that must be taken into account to fully understand the exchange interaction between two magnetic centres.

References

[1] H. Tamaki, Z. J. Zhong, N. Matsumoto, S. Kida, M. Koikawa, N. Achiwa, Y. Hashimoto, H. Okawa, *J. Am. Chem. Soc.* 1992, **114**, 6974.
[2] M. Gruselle, C. Train, K. Boubekeur, P. Gredin, N. Ovanesyan, *Coord. Chem. Rev.*, 2006, **250**, 2491.
[3] C. Train, R. Gheorghe, V. Krstic, L.-M. Chamoreau, N.S. Ovanesyan, G. L. J. A. Rikken, M. Gruselle, M. Verdaguer, *Nat. Mater.*, 2008, **7**, 729.
[4] C. Train, T. Nuida, R. Gheorghe, M. Gruselle, S. Ohkoshi, *J. Am. Chem. Soc.* 2009, **131**, 16838.
[5] A. Alberola, E. Coronado, C. Gimenez-Saiz, C. J. Gomez-Garcia, F. M. Romero, A. Tarazon, *Eur. J. Inorg. Chem.* 2005, 389.
[6] D. Armentano, G. De Munno, F. Lloret, M. Julve, *CrystEngComm* 2005, **7**, 57.
[7] H. Ōkawa, A. Shigematsu, M. Sadakiyo, T. Miyagawa, K. Yoneda, M. Ohba, H. Kitagawa *J. Am. Chem. Soc.* 2009, **131**, 13516.
[8] E. Pardo, C. Train, G. Gontard, K. Boubekeur, O. Fabelo, H. Liu, B. Dkhil, F. Lloret, K. Nakagawa, H. Tokoro, S-I. Ohkoshi, M. Verdaguer *J. Am. Chem. Soc.,* 2011, **133**, 15328.
[9] E. Pardo, C. Train, H. Liu, L-M. Chamoreau, B. Dhkil, K. Boubekeur, F. Lloret, K. Nakatani, H. Tokoro, S-I. Ohkoshi, M. Verdaguer *Angew. Chem., Int. Ed.*, 2012, **51**, 8356.
[10] C. Maxim, S. Ferlay, H. Tokoro, S. Ohkoshi, C. Train, *Chem. Commun.*, 2014, **50**, 5629
[11] C. Maxim, S. Ferlay, C. Train, *New J. Chem.* 2011, **35**, 1254
[12] E. Pardo, C. Train, R. Lescouëzec, K. Boubekeur, E. Ruiz, F. Lloret, M. Verdaguer, *Dalton Trans*., 2010, 39**,** 4951
[13] E. Pardo, C. Train, K. Boubekeur, G. Gontard, J. Cano, F. Lloret, K. Nakatani, M. Verdaguer, *Inorg. Chem.* 2012, **51**, 11582.
[14] E. Coronado, J. R. Galan-Mascaros, C. Martı-Gastaldo, A. M. Martinez *Dalton Trans.*, 2006, 3294-3299
[15] C. Paraschiv, S. Ferlay, M. W. Hosseini, N. Kyritsakas J-M. Planeix, M. Andruh, *Rev. Roum. Chim.*, **2007**, *52*, 101.
[16] S. Ferlay, M. W. Hosseini, in Functional Supramolecular Architectures for Organic Electronics and Nanotechnology, ed. P. Samori, F. Cacialli, Wiley-VCH, 2010.
[17] a) C. Paraschiv, S. Ferlay, V. Bulach and J-M. Planeix, *Chem. Commun.*, 2004, 2270 b) P. Dechambenoit, S. Ferlay, B. Donnio, D. Guillon and M. W. Hosseini, *Chem. Commun.*, 2011, 47, 734; c) Marinescu, G.; Ferlay, S.; Kyritsakas N.; Hosseini, M. W. *Chem. Commun.*, 2013, 11209
[18] J. M. Baylar and E. M. Jones in Inorganic Synthesis; Ed: H. S. Booth, McGraw-Hill, New York, 1939.
[19] P. Dechambenoit, S. Ferlay, N. Kyritsakas, M. W. Hosseini *J. Am. Chem. Soc.* 2008, **130**, 17106.
[20] P. Dechambenoit, S. Ferlay, N. Kyritsakas, M. W. Hosseini *N. J. Chem.* 2010, **34**, 1184.
[21] G. M. Sheldrick, Programs for the Refinement of Crystal Structures, University of Göttingen, Göttingen, Germany, 1996.
[22] A. L. Spek, *J. Appl. Crystallogr.* 2003, **36** ,7.
[23] a) C. J. Calzado, J. Cabrero, J.-P. Malrieu, R. Caballol, *J. Chem. Phys.* 2002, **116**, 2728–2747; b) C. J. Calzado, J. Cabrero, J.-P. Malrieu, R. Caballol, *J. Chem. Phys*. 2002, **116**, 3985–4000.
[24] a) J.-B. Rota, L. Norel, C. Train, N. Ben Amor, D. Maynau, V. Robert, *J. Am. Chem. Soc.* 2008, **130**, 10380; b) J.-B. Rota, C. J. Calzado, C. Train, V. Robert, *J. Chem. Phys.* 2010, **132**, 154702.
[25] J. Miralles, J.-P. Malrieu, R. Caballol, *Chem. Phys.* 1991, **153**, 25–37.
[26] N. Ben Amor, D. Maynau, *Chem. Phys. Lett.* 1998, **286**, 211–220.
[27] J.-P. Malrieu, R. Caballol, C. J. Calzado, C. de Graaf, N. Guihéry, *Chem. Rev.* 2014, **114**, 429–492.
[28] J.-P. Malrieu, N. Guihery, C. J. Calzado, C. Angeli, *J. Comput. Chem.* 2007, **28**, 35.
[29] A. Domingo, C. Angeli, C. Graaf, V. Robert. *J. Comput. Chem.* 2015, **11**, 861.
[30] E. Bordas, R. Caballol, C. de Graaf, J-P. Malrieu, *Chem. Phys.*, 2005, **309**, 259 – 269.
[31] MOLCAS The Next Generation, *J. Comput. Chem.* 2010, **31**, 224-247.
[32] D. Casanova, P. Alemany, J. M. Bofill, S. Alvarez, *Chem. Eur. J.* 2003, **9**, 1281–1295.
[33] M. D.Ward, *Chem. Commun.*, 2005, 5838.
[34] A. Herpin. Théorie du Magnétisme (Presses Universitaires de France, Paris, 1968).
[35] S.I. Ohkoshi, K. Hashimoto, *Phys. Rev. B*, 1999, 60, 12820.
[36] M. Julve, M. Verdaguer, A. Gleize, M. Philoche-Levisalles, O. Kahn, *Inorg. Chem*. 1984, **23**, 3808.
[37] (a) Z. Tabookht, X. López, M. Bénard, C. de Graaf, *J. Phys. Chem. A*, 2010, **114**, 12291–12298. (b) R. Bastardis, N. Guihéry, C. de Graaf, *Phys. Rev. B*, 2007, **76**, 132412.
[38] a) M. Kepenekian, B. Le Guennic, V. Robert *Phys. Rev.* B 2009, **79**, 094428; b) M. Kepenekian, B. Le Guennic, V. Robert, *J. Am. Chem. Soc.* 2009, **131**, 11498-11502.
[39] B. Le Guennic, N. Ben Amor, D. Maynau, V. Robert *J. Chem. Theo. Comp*. 2009, **5**, 1506.
[40] R. Maurice, R. Bastardis, C. de Graaf, N. Suaud, T. Mallah, N. Guihéry, *J. Chem. Theory Comput.*, 2009, **5**, 2977– 2984.
[41] (a) Kahn, O. *Molecular Magnetism*, VCH, New York (1993). (b) Boča, R. *Theoretical Foundations of Molecular Magnetism*, Elsevier, Amsterdam (1999).
[42] R. Maurice, N. Guihéry , R. Bastardis, C. de Graaf, *J. Chem. Theory Comput.* 2010, **6**, 55-65.

[43] L. O. Atovmyan, G. V. Shilov, R. N. Lubovskaya, E. I. Zhilyaeva, N. S. Ovanesyan, S. I. Pirumova, I. G. Gusakovskaya, Y. G, Morozov, *JETP Lett.* 1993, **58**, 766.